Colloid Polym Sci (2008) 286:1265–1272
DOI 10.1007/s00396-008-1887-x

ORIGINAL CONTRIBUTION

Self-assembled films of cellulose nanofibrils and poly(*o*-ethoxyaniline)

Eliton S. Medeiros · Luiz H. C. Mattoso · Rubens Bernardes-Filho · Delilah F. Wood · William J. Orts

Received: 14 April 2008 / Revised: 6 May 2008 / Accepted: 8 May 2008 / Published online: 15 July 2008

Abstract Nanostructured films of poly(o-ethoxyaniline) (POEA) alternated with cellulose nanofibrils (CnF) were successfully produced by self assembly (SA) at different pH values and investigated by atomic force microscopy and ultraviolet-visible spectroscopy. Results show that it was possible to build up films by alternating POEA and CnF layers with relatively precise architectural control by controlling the number of layers and pH. Film thickness had a dependence on pH which is a combination of the effects of the deposited amount for each POEA layer and the pH at which the absorption of the cellulose nanofibrils was carried out. Comparison of alternated layers of POEA and CnF with multi-immersions of POEA at different pH values, as measured by the ratio between slopes of the straight lines of deposited amount of polymer versus the number of self-assembled layers, shows that alternate deposition at pH 2 has a fourfold increase in the slope. Alternatively, at pH 5, there is no significant difference whether the deposition is alternated (POEA–CnF) or not (POEA).

Keywords Cellulose nanofibrils · Poly(*o*-ethoxyaniline) · Conducting polymers · Self-assembly

E. S. Medeiros · L. H. C. Mattoso · D. F. Wood · W. J. Orts (✉)
United States Department of Agriculture,
Bioproduct Chemistry and Engineering Unit,
Western Regional Research Center,
800 Buchanan St.,
Albany, CA 94710, USA
e-mail: bill.orts@ars.usda.gov

E. S. Medeiros · L. H. C. Mattoso · R. Bernardes-Filho
Laboratório Nacional de Nanotecnologia para o Agronegócio,
Embrapa Instrumentação Agropecuária,
Rua XV de Novembro, 1452,
São Carlos 13560-970, Brazil

Introduction

Although cellulose nanofibrils (also known as microcrystalline cellulose, cellulose whiskers, nanofibrils, and nanocrystals) have been studied and industrially used since early 1960s [1–3]; these nanostructures have gained more scientific attention only recently due to the search for nanomaterials from renewable resources. Moreover, cellulose is the most abundant form of biomass with an estimated annual production of 1.5×10^{12} ton [4–7], and its nanofibrils exhibit remarkable physical and rheological properties [6, 8, 9].

Similarly, conducting polymers have gained more scientific attention over the last two decades because of their unique combination of properties of both metals and plastics, which has enabled applications in devices such as sensors and biosensors [10], batteries [11], light emitting diodes and electroluminescent displays [12, 13], and coatings [6, 14, 15]. In most of these applications, the polymer is used in the form of thin films which are usually produced by self assembly, spin coating, Langmuir-Blodgett, or casting [16–18]. Therefore, control of film architecture is of paramount importance to attaining film reproducibility, durability, and performance.

Self-assembly has been used to build up multilayered films by means of electrostatic attraction forces, stereocomplex formation, host–guest interactions, and hydrogen and covalent bonds [16]. This has allowed different types of materials to be assembled into thin films with a relatively precise control of architecture by adjusting process conditions such as nature and concentration of materials, pH, ionic strength, immersion time, dopant counter-ion, and number of layers. Furthermore, self-assembly offers several advantages over other techniques used for thin film formation since the substrate can take any form and size,

the deposition time is independent of the substrate area, and there are no requirements for additional equipments and/or clean rooms [17–21].

In this work, nanostructured multilayer thin films of poly (*o*-ethoxyaniline) and cellulose nanofibrils were successfully produced by self-assembly at different pH values, and their structure was investigated by atomic force microscopy (AFM) and ultraviolet-visible (UV-Vis) spectroscopy.

Experimental

Polymer synthesis and characterization

Poly(*o*-ethoxyaniline) was chemically synthesized using freshly distilled *o*-phenetidine (1.0 M, Sigma Aldrich). Ammonium persulfate (APS; 0.25 M, Mallinckrodt) and hydrochloric acid (HCl; 1.0 M, Fischer Chemicals) were used as oxidant and dopant, respectively. The monomer to oxidant ratio was kept at 4:1 with polymerization carried out at room temperature for about 3 h.

The polymerization was monitored by measuring the open-circuit potential (V_{oc}) of the reaction using a platinum (working) electrode versus a saturated calomel (reference) electrode (SCE). Subsequently, the poly(*o*-ethoxyaniline) (POEA) powder obtained was removed from reaction medium, filtered under vacuum, exhaustively rinsed with acetone to remove unreacted monomers and oligomers, and dried in vacuum for 24 h.

Fourier transform infrared spectroscopy (FTIR) analysis of the polymer was recorded on a Perkin-Elmer 1000 IR spectrometer, spectral window ranging from 400 to 4,000 cm^{-1} and resolution of 4 cm^{-1}. Samples were prepared using KBr pellets containing about 2 wt.% of the polymer powder. UV-Vis spectra were recorded on a Shimadzu UV-Visible spectrophotometer model UV 1700 PharmaSpec from 200 to 1,100 nm.

Extraction of cellulose nanofibrils

Extraction of cellulose nanofibrils was carried out according to the methodology described by Favier et al. [22]. Briefly, 10% *w*/*v* short cellulose fibers (Fibrous cellulose powder CF11, Whatman Int. Ltd., England) was stirred vigorously with 60 wt.% sulfuric acid preheated and maintained at 60 °C for 45 min. The mixture was, then, quenched in cold water and stirred. The resulting dispersion was centrifuged, decanted, and washed with water continuously until the pH was above 1.5 and a stable dispersion formed. The resulting solution was water dialyzed in dialysis tubing (Spectrapor 2; MWCO 12,000–14,000; 45 mm flat width) for 4–5 days until the pH of the solution was between 5.5 and 6.5. Cellulose nanofibrils were recovered as a dispersion of approximately 1.16 g/100 mL water from dialysis.

Preparation of solutions of POEA and nanofibrils

POEA solutions were prepared by dissolution of POEA in deionized water under stirring for overnight. The final concentration of polymer was c.a. 1.0×10^{-3} mol L^{-1} (0.611 g L^{-1}), based on its doped tetramer (see Scheme 1) and the pH of each solution was adjusted to 2, 3, 4, and 5 using 1.0 M HCl and/or 0.1 M NH_4OH solutions.

The dispersion of cellulose nanofibrils was diluted to make 0.611 g L^{-1} solutions whose pH values were also adjusted to 2, 3, 4, and 5 using 1.0 M HCl and/or 0.1 M NH_4OH solutions.

Film growth and characterization

Glass slides (10×10×1 mm) used for film deposition were previously cleaned with hot *piranha* solution, H_2SO_4/H_2O_2 (7:3 *v*/*v*), for 1 h and $H_2O/H_2O_2/NH_4OH$ (5:1:1 *v*/*v*) solution for 30 min. In each step of the cleaning process, these slides were extensively rinsed with deionized water.

Films were deposited by self-assembly onto glass slides using the polymer solutions with pH adjusted as previously described. The isosbestic points of POEA (HCl) in water were determined by UV-Vis spectrophotometry from 10^{-3} M POEA solutions at different pH values and the kinetics of adsorption was carried out by measuring the absorbance at 455 nm for fixed periods of time, ranging from 0 up to 30 min, until absorbance reached a constant value.

The amount of material adsorbed, Γ (μg/cm^2), was calculated according to the Beer-Lambert law, which

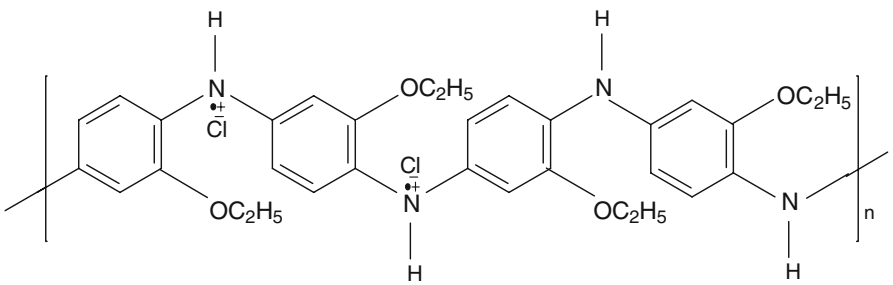

Scheme 1 Chemical structure of a repeating HCl-doped tetramer that constitutes poly (*o*-ethoxyaniline)

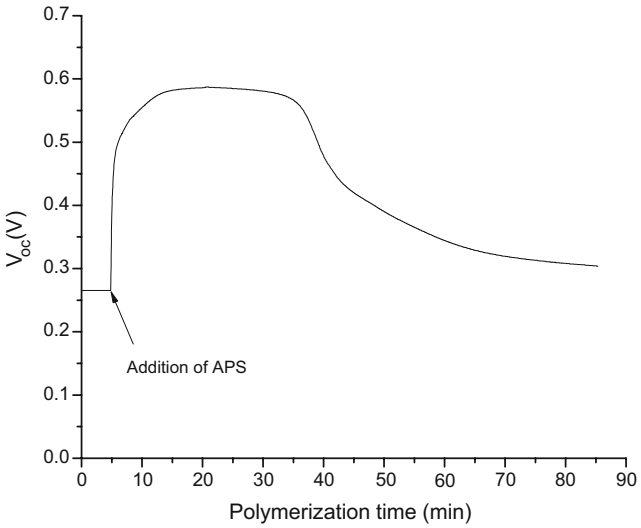

Fig. 1 Open circuit potential of (Voc in Volts versus SCE) as a function of polymerization time for POEA, indicating the addition of APS to the aniline solution, both in aqueous 1 M HCl

provides a relationship between absorbance, A (a.u.), molar absorptivity ε (m^2/g), path length b (mm), and molar concentration c (g/L) by

$$A = b\varepsilon_i c_i$$

where the subscript i refers to poly(*o*-ethoxyaniline) or cellulose nanofibrils (CnF).

Based on the kinetic studies, both POEA and POEA alternated by CnF (POEA–CnF) films were built up according to the following procedure: (1) deposition of a POEA layer for 10 min; (2) rinsing for 15 s in deionized water at the same pH of the deposition polymer solution to remove loosely adsorbed polymer chains; (3) drying gently with a nitrogen flow; (4) measurement of film absorbance at 455 nm by UV-Vis spectrophotometry; and (5) deposition of a CnF layer followed by the rinsing (step 2) and drying (3) steps. For multi-immersion films of POEA only steps 1 through 4 were repeated, whereas POEA–CnF multi-layered films were assembled by repeating steps 1 through 5. In each case, films containing ten layers (monolayers for POEA and bilayers for POEA–CnF films) were produced.

AFM Characterization

AFM images of the top layer of self-assembled films with ten immersions of POEA and ten bilayers of POEA–CnF were obtained with a Topometrix TMX 2010 Discoverer Atomic Force Microscope in the noncontact mode, using probes with a nominal tip radius of 20 nm and a spring constant of 5 N/m. The obtained images were processed using Gwydion© 2.1 data analysis software. Line profile analyses of AFM images also enabled determination of nanofibril dimensions.

Results and discussion

Figure 1 shows V_{oc} as a function of the polymerization time of POEA using a two-electrode configuration. It can be observed that there is a steep increase in V_{oc} immediately after addition of APS to monomer in acidic medium, followed by a maximum (0.59 V, SCE) between 15 and 35 min, and then a decrease to around 0.32 V due to the completion of the polymerization reaction after approximately 70 min. The peak, with maximum of about 0.59 V, is associated with pernigraniline oxidation state, which is the fully oxidized state of polyaniline and derivatives. According to the literature, pernigraniline acts as an oxidizing agent to remaining monomers and oligomers, while being itself reduced to the half-oxidized emeraldine oxidation state [23–25]. In this stage, V_{oc} decays and the polymer formed precipitates as a dark green-colored powder, characteristic of the doped emeraldine salt state.

The FTIR spectrum of as-synthesized POEA/HCl powder in Fig. 2 displays absorption peaks characteristic of polyaniline in the emeraldine HCl-doped state. This result is in accordance with those reported in the literature [26–29] as described below. The absorption peaks between 3,450 and 2,950 cm^{-1} are assigned to symmetric H stretching of the N–H and C–H bondings; the peaks at 1,490 and 1,560 cm^{-1} are assigned, respectively, to symmetric C=C stretching of the quinoid and benzenoid aromatic rings; the peaks at 1,260 and 1,135 cm^{-1} are assigned to $(C–N)^+$ symmetric stretching of secondary amines bonded to aromatic groups and $–NH^+=$, therefore, indicating that the polymer is in its doped form; and absorption peaks at 1,400 and 1,300 cm^{-1} are, respectively, attributed to in-plane angular stretching of C–H and C–N of secondary amines bonded to aromatic rings. The region between 1,245 and 1,030 cm^{-1}, respectively assigned to symmetric and asymmetric stretching of the C_{ar}–

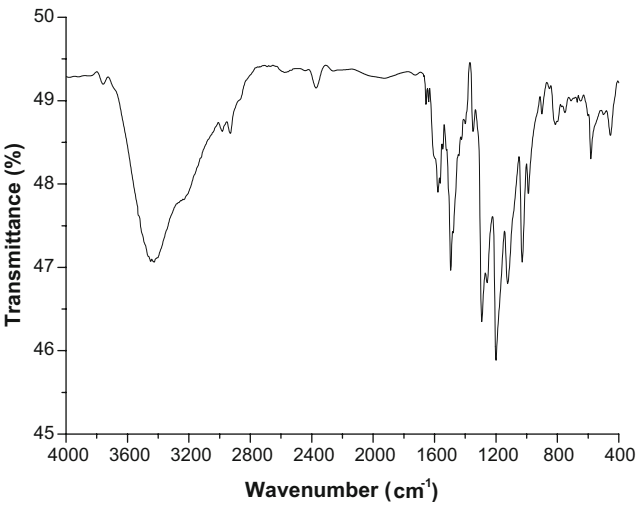

Fig. 2 FTIR spectrum of the as-synthesized POEA–HCl powder

O–C (ar = aromatic), is characteristic of o-ethoxy groups of POEA; the region between 800 and 450 cm^{-1} is characteristic of 1,4-disubstituted benzene rings, indicating that growth of polymer chains is predominantly linear.

The UV-Vis spectra of POEA in water at various pH values are shown in Fig. 3. These spectra show three absorption bands whose wavelength of the peak maxima depend on pH, e.g., for pH 3, these maxima are located at approximately 350, 430, and 740 nm. The absorption at 350 nm is characteristic of π→π* electronic transitions of the benzenoid rings of POEA; the absorptions bands at 430 and 740 nm are associated with excitonic (n→π*) transitions (electronic transitions from the highest occupied molecular orbitals (HOMO) of the benzenoid rings to lowest unoccupied molecular orbitals (LUMO) of the localized quinoid rings) of the polarons [30]. The peak at 740 nm shifts toward lower wave numbers with increasing pH due to the decrease in doping level. This reduces both the intensity of the polaronic band and the number of polarons. These spectra also show two isosbestic points at 374 and 455 nm. The isosbestic point at 455 nm was used to monitor the adsorption of POEA and POEA alternated with CnF.

Figure 4 shows the graph of the amount of adsorbed material (Γ) versus deposition time (t) for the first layer of POEA at pH 2, 3, 4, and 5. These results show that both the stabilization time for the deposition of the first layer and the amount of polymer deposited depend on solution pH. Since more than 90% of the adsorbed amount is deposited in the first 10 min of immersion, as observed by the decrease in slope of the Γ vs. t curve, this value was chosen as the deposition time to be used for building multilayered films. The longer stabilization time required for the highest and lowest pH investigated (pH 5 and 2) is, respectively, due to the lower attraction forces between weakly charged molecules and the substrate and electrostatic repulsion

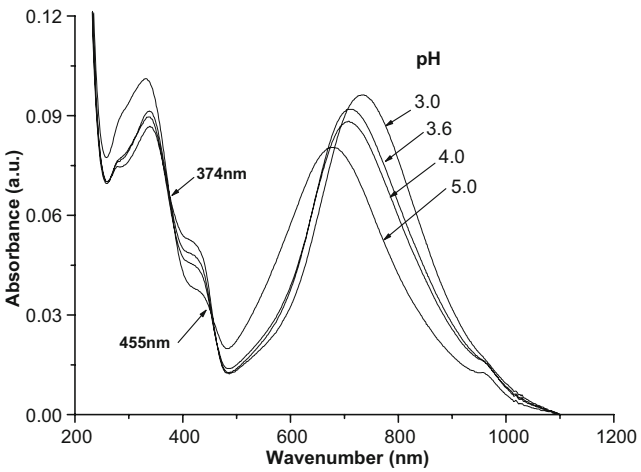

Fig. 3 UV-Vis spectra of POEA/HCl in water at different pH, as indicated, showing two isosbestic points at 374 and 455 nm

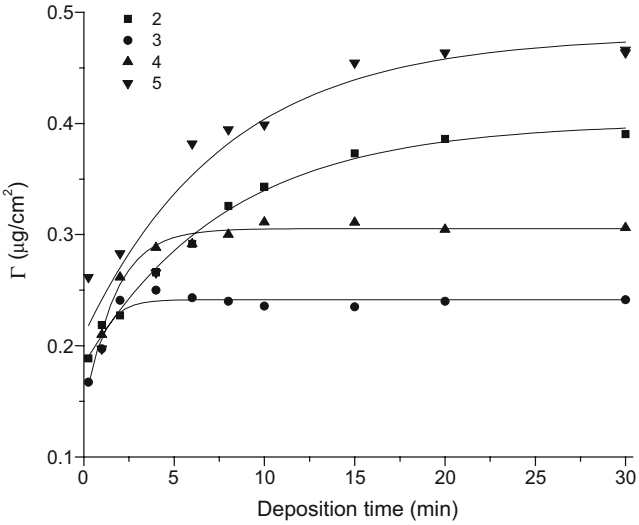

Fig. 4 Amount of adsorbed material as a function of deposition time for 10^{-3} M POEA at pH 2, 3, 4, and 5

forces between highly charged POEA molecules, which prevent a faster diffusion of the polymer chains from the bulk solution to the substrate. Nevertheless, by keeping the immersion time fixed for each layer, one may assure that each immersion contributes with approximately a same amount of polymer, as it will be shown later.

Polymer molecules can assume different conformations depending on factors such as pH, backbone rigidity, concentration, and polymer–solvent interactions [31–35]. At lower pH values, polyelectrolyte molecules assume an extended or rod-like conformation as a consequence of the electrostatic repulsion forces between doped sites within the same polymer backbone, whereas at higher pH, they can assume a coiled conformation as a result of the lower electrostatic repulsion forces [36]. When a polymer is adsorbed on a surface charged with oppositely charged sites, it may neutralize the charges on the surface or even overcompensate for them [37, 38].

The number of charged sites of a molecule which can interact with an oppositely charged layer is dependent on pH and chain flexibility. Thus, the driving forces for deposition are a balance of (1) attraction forces, specifically between charged molecules and the oppositely charged substrate, (2) repulsion forces between polymer chains with the same type of charge, and (3) chain conformation and flexibility that depends on pH, as previously mentioned. Therefore, rather than a linear trend of increasing thickness with pH, there is a small range of pH in which the thickness reaches a maximum value. This occurs when the surface charge density experienced by an adsorbing, fully charged polyelectrolyte drops below the critical value needed to overcome chain coiling entropy effects [16, 22].

Figure 5 shows the growth for ten layers of POEA (a) and POEA–CnF (b) self-assembled films as a function of

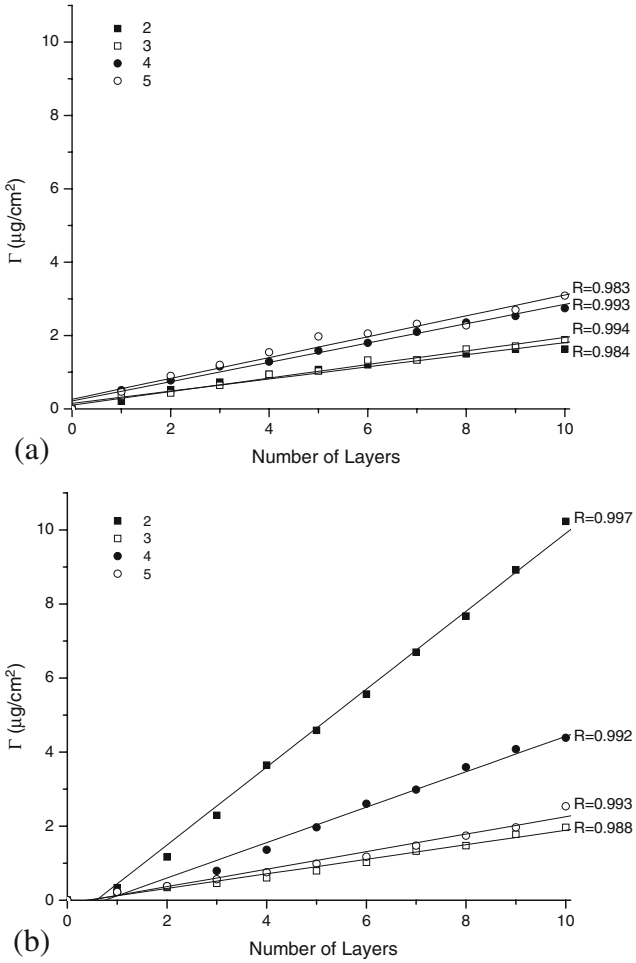

Fig. 5 Amount of adsorbed material as a function of the number of (**a**) POEA layers and (**b**) POEA–CnF bilayers measured at 455 nm, and at pH 2, 3, 4, and 5

pH. It can be observed that the amount of material deposited for POEA alternated with CnF is much greater than that for POEA alone, indicating that CnF is also being alternately deposited at the various pH investigated. When multilayer films of POEA are built up, the amount of polymer deposited has a linear dependence with pH so that the more acidic the polymer (higher doping level), the lower the amount of deposited polymer (after forming a relatively uniform first layer on the glass substrate). This occurs because, at lower pH, POEA is a polycation whose positively charged molecules are repulsed by each other. In this case, strong repulsive forces slow down the rate of film growth, leveling off when the driving forces for adsorption approach equilibrium with repulsive ones. The amount of material deposited, and consequently the thickness of deposited layers, depends also on factors such as polymer concentration, type of dopant and ionic strength of the solution [39–47].

Another important feature observed is that each POEA–CnF bilayer contributed to an approximately equal amount of deposited material, indicated by the correlation of the straight lines (R^2>0.97) from the plot of amount of POEA adsorbed as a function of the number of (bi)layers deposited (Fig. 5). Straight lines imply that regular multilayers were obtained. The deviation from linearity for two or three first layers is due to influence of the nature of substrate and polyelectrolytes involved in the adsorption process; linear growth is reached only after this zone. This behavior can be explained by the zone model for film growth proposed by Ladam et al. [48] and Pointu et al. [49] in which multilayer films are subdivided into three distinct zones. The first zone, which is comprised of one or a few polyelectrolyte layers close to the substrate, is influenced by the nature of the substrate; the third zone, which is comprised of one or more polyelectrolyte layers close to the surface of the film can be influenced by the interface to the solution or to air; and the second zone, which is not influenced by the interfaces and has more uniform properties [16]. In subsequent layers, film growth is relatively uniform and each bilayer should preferably contribute to an equal amount of material to the film being formed.

The ratios between slopes of the straight lines of Γ versus number of (bi)layers of self-assembled films of POEA–CnF and POEA, $n_{(POEA–CnF)}/n_{(POEA)}$, calculated as shown in Fig. 6 for pH 2, give an idea of how efficient alternate adsorption of POEA–CnF is compared to multi-immersions of POEA. The values of $n_{(POEA–CnF)}/n_{(POEA)}$ for pH 2, 3, 4, and 5 presented in Table 1 show that the amount of POEA deposited when alternated with CnF can be as high as 4.9±1.4 times the amount of multi-immersions of POEA, suggesting that it was possible not only to assemble alternate multilayered films of POEA and CnF but also to control their thickness by controlling both pH and number of layers. Furthermore, a closer inspection of Fig. 6 shows that instead of each immersion of POEA contributing with the same amount of

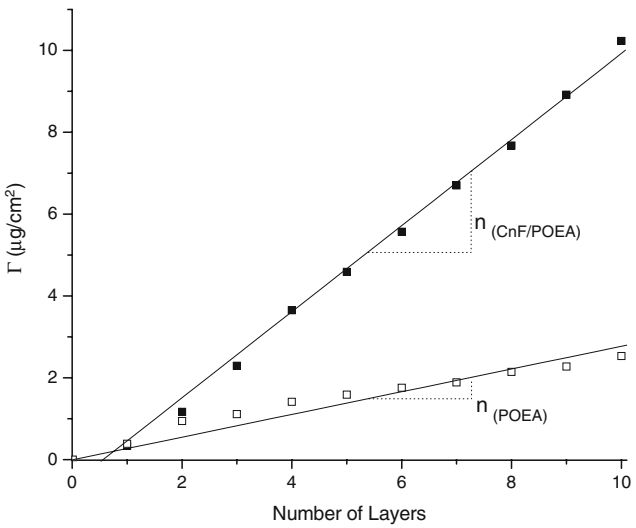

Fig. 6 Amount of adsorbed material as a function of the number of layers (POEA–CnF or POEA) measured at 455 nm and pH 2

Table 1 Ratio between slopes of the straight lines of Γ vs. number of (bi)layers of self-assembled films of POEA–CnF ($n_{(POEA–CNF)}$) and POEA ($n_{(POEA)}$) as a function of pH

pH	$n_{(POEA–CnF)}/n_{(POEA)}$
2	4.9±1.4
3	1.2±0.2
4	2.0±0.3
5	0.9±0.2

polymer (when only POEA is being deposited), there is a trend for the layer growth to stop after complete charge compensation, which normally occurs after a certain number of immersions and depends on polymer backbone rigidity, dopant counter ion, solvent, and solution pH.

Contrary to POEA growth, whose thickness of self-assembled layers increased with decreasing pH, alternated layers of POEA and cellulose nanofibrils (POEA–CnF) do not follow the same trend. Acid hydrolysis removes flexible amorphous sections linking cellulose crystals to form nanofibrils of about 10 to 50 nm in diameter and an average aspect ratio between 10 and 100 [1, 4]. As a result, these nanofibers have electronegative surface charges on their surface (usually sulfate and polar hydroxyl groups) that are capable of hydrogen bonding, leading to particle–particle or particle–solvent–particle interactions to form three-dimensional networks [1–3, 50–52]. Consequently, changes in pH affect not only optical and rheological properties of cellulose nanofibrils but also the formation of self-assembled thin films by changing interaction forces between nanofibrils and, thus, preventing their diffusion from the solution to the growing films.

The effect of pH on rheological properties of cellulose nanofibrils dispersions was studied by Yaginuma and Kijima [39]. The authors reported that 0.3 wt.% aqueous dispersions of fine particles showed solid-like dynamic viscoelastic behavior at low pHs (below pH 3), in contrast to liquid-like behavior at high pHs. This suggests that, at lower pH, electrostatic repulsion forces between cellulose nanofibrils decrease to induce aggregation of particles into a three-dimensional network structure as pointed out by Battista et al. [1–3]. A similar behavior was also observed by Ono et al. [53, 54] with aqueous suspensions of cellulose nanofibrils in which both viscosity and relative transmittance (optical transparency) of these suspensions

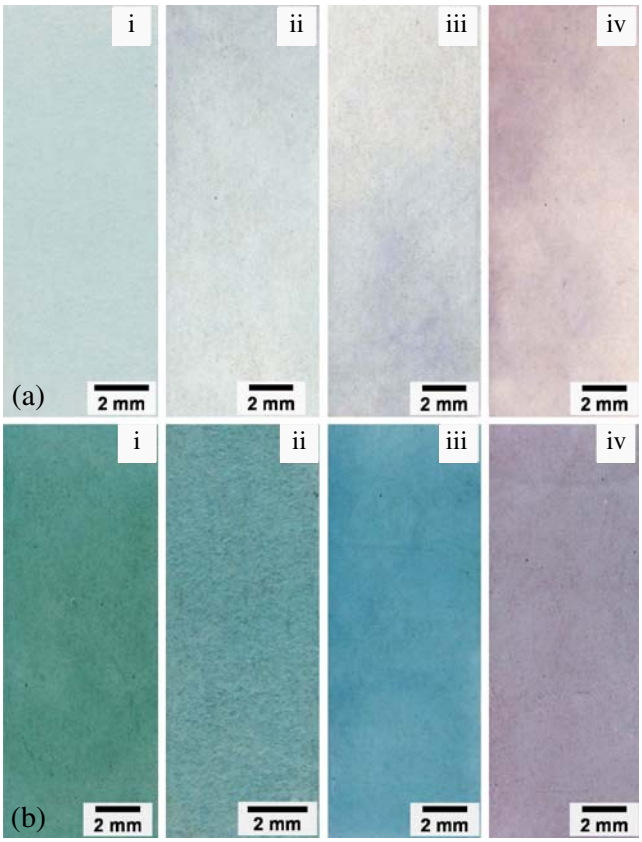

Fig. 7 Photographs of self-assembled thin films of (**a**) POEA and (**b**) POEA–CnF deposited on glass slides at pH 2 (*i*), 3 (*ii*), 4 (*iii*), and 5 (*iv*)

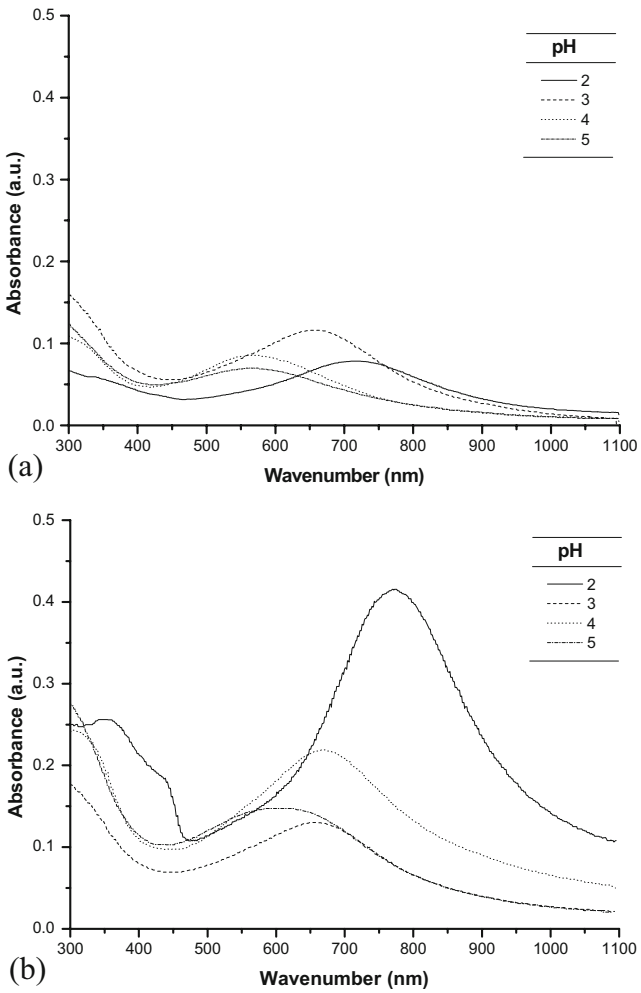

Fig. 8 UV-Vis spectra of (**a**) POEA and (**b**) POEA–CnF self-assembled films deposited at pH 2, 3, 4, and 5

were abruptly changed at lower and higher pH regions, whereas, at intermediate pH values, changes in pH had little effect on viscosity and optical transparency.

Consequently, the thickness of each POEA–CnF bilayer depends not only on factors which control the deposition of polyelectrolytes, as previously discussed, but also on pH dependence of viscosity of CnF suspensions. Changes in viscosity can decrease or eventually prevent diffusion of nanofibrils from solution to the film being assembled. Moreover, film thickness had a dependence on pH ($l_2 > l_4 > l_5 > l_3$, where l_i = film thickness at pH i) which is a combination of the effects of the deposited amount for each POEA layer ($l_5 > l_2 > l_4 > l_3$) and the pH at which the absorption of the cellulose nanofibrils was carried out ($A_2 > A_4 > A_5 > A_3$, where A_i = absorbance at pH i).

Figures 7 and 8 show, respectively, images of films deposited onto glass slides and UV-Vis absorption spectra of POEA and POEA–CnF self-assembled films deposited at pH 2, 3, and 4.

It is possible to observe in Fig. 7 that the color intensity and, therefore, film thickness is much higher for POEA–CnF films than for plain POEA films. Furthermore, as pH decreases, film color changes from light blue to bluish-green and then green, which are characteristic colors expected for increasing doping level of this polyaniline derivative [13, 23, 24, 26]. UV-Vis spectra of Fig. 8 show that the polaronic band shifted according to pH changes; also, in conformity with Fig. 3 and the absorbance values of POEA–CnF, self-assembled films deposited at pH 2, 3, 4, and 5 are superior to those on multi-immersions of POEA as already pointed out.

AFM images of the top layer of POEA and POEA–CnF films shown in Fig. 9 confirm the presence of CnF within POEA–CnF self-assembled films investigated.

Figure 9 shows that a globular morphology was obtained for plain POEA films [36, 37], whereas a typical fibrillar morphology was observed for the films containing cellulose nanofibrils. Moreover, image analysis shows that these fibers have an average diameter (d) of 38±13 nm, length (l) of 360±60 nm, and aspect ration (l/d) of 10±4 nm, therefore, in agreement with the literature [8, 55, 56]. These results confirm that multilayered thin films of POEA

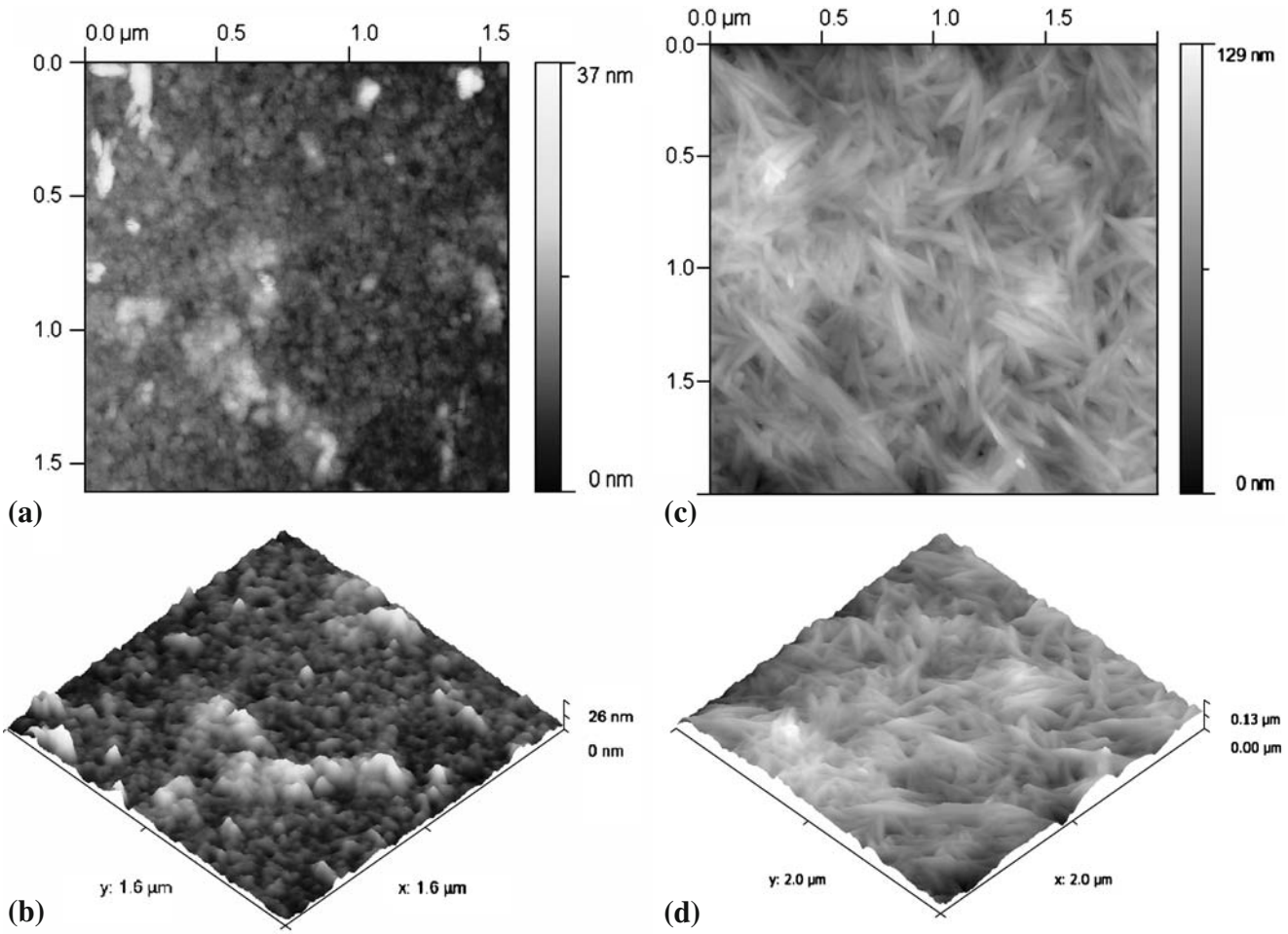

Fig. 9 2D and 3D AFM images of self-assembled thin films showing the top layer (tenth immersion of POEA or tenth bilayer of POEA–CnF) of POEA (**a**, **b**) and POEA–CnF (**c**, **d**)

and CnF could be successfully produced at different pH under the conditions investigated.

Conclusions

Nanostructured films of POEA alternated with CnF were successfully produced by self-assembly, showing that cellulose nanofibrils can be assembled to build up multilayer thin films in a similar way to polyelectrolyte deposition. These films exhibited a relatively precise control of the architecture by controlling the deposition conditions, since a constant amount of material can be adsorbed in each immersion allowing the build-up of multilayered films. Alternated layers of POEA and CnF can present up to a four-fold increase in the amount of material deposited (at pH 2) when compared to multi-immersions of POEA. This behavior is a result of the dependence of POEA–CnF bilayers with the factors that control the deposition of polyelectrolytes and pH dependence of viscosity of CnF suspensions. The thickness of each POEA–CnF bilayer depends on the solution pH and the resulting electrostatic attraction forces. Such nanostructured composites might find interesting applications, including sensors, biomedical materials and electrochromic devices.

Acknowledgements One of the authors, Luiz H. C. Mattoso, would like to acknowledge CNPq and Embrapa/Labex program for their support to this research.

References

1. Battista OA, Smith PA (1962) Ind Eng Chem 54:20, doi:101021/ie50633a003
2. Battista OA, Erdi NZ, Ferraro CF, Karasinski FJ (1967) J Appl Polym Sci 11:481, doi:10.1002/app.1967.070110401
3. Battista OA (1975) Microcrystalline polymer science. McGraw-Hill, New York
4. Deguchi S, Tsujii K, Horikoshi K (2006) Chem Commun 31:3293
5. Crawford RL (1981) Lignin biodegradation and transformation. Wiley, New York
6. Klemm D, Heublein B, Fink H-P, Bohn A (2005) Angew Chem Int Ed 44:3358, doi:10.1002/anie.200460587
7. Kima IS, Kimb JP, Kwakb SY, Koc YS, Kwonc YK (2006) Polymer 47:1333
8. Orts WJ, Shey J, Imam SH, Glenn GM, Guttman ME, Revol J-F (2005) J Polym Environ 3:301, doi:10.1007/s10924-005-5514-3
9. Marcovich NE, Auad ML, Bellesi NE, Nutt SR, Aranguren MI (2006) J Mater Res 21:870
10. Medeiros ES, Paterno LG, Mattoso LHC (2006) In: Grimes CA, Dickey EC, Pishko MV (eds) Encyclopedia of sensors. vol. X. American Scientific, Stevenson Ranch, pp 1–36
11. Bullock SE, Kofinas P (2004) J Power Sources 132:256, doi:10.1016/j.jpowsour.2003.12.045
12. Saxena V, Malhotra BD (2003) Curr Appl Phys 3:293
13. Heeger AJ (2001) MRS Bulletin 900
14. Tang Z, Kotov NA (2005) Adv Materials 17:951
15. Malinauskas A (2001) Polymer 42:3957
16. Decher G (2003) In: Decher G, Schlenoff JB (eds) Multilayer thin films, Chapter 1. Wiley, Weinheim, pp 1–46
17. Rubner MF (2002) In: Decher G, Schlenoff JB (eds) Multilayer thin films, Chapter 5. Wiley, Weinheim, pp 133–154
18. Harsányi G (1995) Sens Actuators A46-47:85
19. Harsányi G (1995) Polymer films in sensor applications. Technomic Publishing, Lancaster
20. Göpel W (1996) Sens Actuators A56:83
21. Li D, Jiang Y, Wu Z, Chen X, Li Y (2000) Sens Actuators B66:125
22. Favier V, Chanzy H, Cavaille JY (1996) Macromol 28:6365
23. Mattoso LHC, MacDiarmid AG (1996) In: Salamone JC (ed) Polymeric Materials Encyclopedia, vol 7. CRC, Boca Raton, pp 5505–5513
24. Cordeiro MAM, Gonçalves D, Bulhões LOS, Cordeiro JMM (2005) Mat Res 8:5
25. Albuquerque JE, Mattoso LHC, Faria RM, Masters JG, MacDiarmid AG (2004) Synth Met 146:1
26. Angelopoulos M, Dipietro R, Zheng WG, MacDiarmid AG (1997) Synth Met 84:35
27. Bhat NV, Seshadri DT, Phadke RS (2002) Synth Met 130:185
28. Tamirisa PA, Liddell KC, Pedrow PD, Osman MA (2004) J Appl Polym Sci 93:1317
29. Stejskal J, Sapurina I, Trchová M, Proneš J (2002) Chem Mat 14:3602
30. Stejskal J, Kratochvil P, Radhakrishnan N (1993) Synth Met 61:225
31. Young RJ, Lovell P (1991) Introduction to polymers, 2nd edn. CRC, Boca Raton
32. Billmeyer FW Jr (1989) Textbook of polymer science, 3rd edn. Wiley, New York
33. Flory PJ (1953) Principles of polymer chemistry. Cornell University Press, Ithaca
34. Morawetz H (1975) Macromolecules in solution. Wiley, New York
35. Yamakawa H (1971) Modern theory of polymer solutions, 2nd edn. Wiley, New York
36. Paterno LG, Mattoso LHC (2001) Polymer 42:5239
37. Paterno LG, Mattoso LHC (2002) J Appl Polym Sci 83:1309
38. Tsukruk VV (1997) Prog Polym Sci 22:247
39. Yaginuma Y, Kijima T, Dispers (2006) J Sci Tech 27:365
40. Zheng HP, Rubner MF, Hammond PT (2002) Langmuir 18:4505
41. Cheung JH, Fou AF, Rubner MF (1994) Thin Solid Films 244:985
42. Raposo M, Mattoso LHC, Oliveira ON Jr (1998) Thin Solid Films 329:327
43. Gardner JW, Varadan VK, Awadelkarim OW (2002) Microsensors, MMS, and smart devices. Wiley, Chichester
44. Rubner MF (2003) In: Decher G, Schlenoff JB (eds) Multilayer thin films. Wiley, Weinheim, p 133–154
45. Borukhov I, Andelman D (1998) Macromol 31:1665
46. Castelnovo M, Joanny J-F (2000) Langmuir 16:7524
47. Rubner MF, Skotheim TA (1991) In: Brédas JL, Silbey R (eds) Conjugated polymers. Kluwer Academic, Dordrecht, p 363
48. Ladam G, Schaad P, Voegel JC, Schaaf P, Decher G, Cuisinier F (2000) Langmuir 16:1249
49. Pointu D, Decher G (2000) Actualites GFP 88:3
50. Roman M, Winter WT (2004) Biomacromol 5:1671, doi:10.1021/bm034519
51. Wang N, Ding E, Cheng R (2007) Polym 48:3486
52. Araki J, Wada M, Kuga S, Okano T (1998) Colloids Surf A142:75
53. Ono H, Shimaya Y, Sato K, Hongo T (2004) Polym J 36:684
54. Ono H, Yamada H, Matsuda S, Okajima K, Kawamoto T, Iijima H (1998) Cellulose 5:231
55. Dong XM, Revol J-F, Gray DG (1998) Cellulose 5:19, doi:10.1002/1521-3765(20010504)7:9
56. Rodriguez NLG, Thielemans W, Dufresne A (2006) Cellulose 13:261